Stochastic modeling for the stress inversion of vein orientations: paleostress analysis of Pliocene epithermal veins in southwestern Kyushu, Japan

Atsushi Yamaji[a], Katsushi Sato[a], Satoshi Tonai[a,b]

[a] *Division of Earth and Planetary Sciences, Graduate School of Science, Kyoto University, Kyoto 606-8502, Japan*
[b] *Present address: National Institute of Advanced Industrial Science and Technology (AIST), Geological Survey of Japan, Tsukuba, Ibaraki 305-8567, Japan*

Abstract

Plio-Pleistocene epithermal quartz veins in southern Kyushu, Japan, include gold deposits. The coherent trend of the ore veins suggests tectonic control for their formation. However, the stress regime during the formation has been controversial. To solve this problem, we improved existing methods for inferring paleostresses from vein orientations. It was assumed that veins making a cluster were formed intermittently from thermal fluids with various pressures. The present method determines stress ratio and stress axes with 95% confidence regions. The method was applied to mid Pliocene quartz veins cropping out at Hashima, southwestern Kyushu. We obtained a normal faulting regime of stress with the trend of sigma3 at 167° ± 10° and the stress ratio at 0.20 +0.13/−0.09. The low stress ratio and the lack of slickenlines and slickenfibers on vein walls suggest that the host rock was subject to a small differential stress, i.e., a weak tectonic stress, when the veins were formed.

Keywords: geothermal fluid, tectonic stress, Bingham distribution, vein-type ore

1. Introduction

Mineral veins are fossils of episodic venting of fluids from deep earth. Understanding of their formation is important not only to mining but also to hydrocarbon exploration (Hood et al., 2003; Sorkhabi, 2005; Tamagawa et al., 2008), geological disposal or storage (Shipton et al., 2004) and earthquake disaster prevention (Sibson, 1987, 2000; Beeler et al., 2000; Miller et al., 2004).

There are Plio-Pleistocene epithermal gold veins in the southern part of Kyushu Island, northern Ryukyu arc, Japan (e.g., Izawa and Urashima, 2001; Izawa and Watanabe, 2001), where most ore veins have coherent trends (Fig. 1). Therefore, following Newhouse (1942) and McKinstry (1948), regional tectonics has been regarded as an important factor for the vein formation (e.g., Shiobara and Yoshikawa, 1958; Ikeda, 1962; Matsutoya, 1967; Sanematsu et al., 2006). However, it has been unclear which stress regime, normal or strike-slip faulting, prevailed in the metallogenic province (Ikeda, 1962; Matsutoya, 1967; Uto et al., 2001; Sillitoe and Hedenquist, 2003; Yamaji, 2003; Yamaji et al., 2003; Hikichi and Yamaji, 2008). To solve this problem, we observed quartz veins at the Hashima site, southwest Kyushu (Fig. 1), where gold-silver deposits were mined until the early 20th Century.

At the beginning of this project, we planned to employ the method of Jolly and Sanderson (1997), which has been applied to veins and dikes in several areas (e.g., Andre et al., 2001; McKeagney et al., 2004; Mazzarini and Isola, 2007; Mazzarini and Musumeci, 2008). The method makes use of vein orientations to infer the paleostress during vein formation. For this purpose, it is expected that poles to veins are oriented in an elliptical cone or along a girdle, and that domains with and with-out data points are clearly separated on a stereogram (Fig. 2a). The σ_3 orientation is, then, determined as the axis of the cone or the densest point on the girdle; and the $\sigma_2\sigma_3$-principal stress plane coincides with the major axis orientation of the ellipse or with the girdle. This method is based on the principle that thermal fluid opens fractures by its pressure, p_f, only if the pressure exceeds the normal stresses on the fractures (Delaney et al., 1986). The Mohr diagram in Fig. 2a illustrates this situation. The domains with and without data points correspond to the orientations whether this condition was satisfied or not. The shape and position of the boundary line between the domains indicate the stress in question. Accordingly, the number density of poles should have an abrupt change across this line to estimate the state of stress.

However, it was difficult to apply the method to our data. Poles to the Hashima veins showed a nebulous pattern on a stereogram (Fig. 2b). Consequently, we improved the methods of Baer et al. (1994) and Jolly and Sanderson (1997) to cope with vein orientations with such a gradation.

2. Stochastic model

2.1. Normalization

The present method aims at determining the state of stress during the formation of veins from their orientations. In general, orientations are dimensionless quantities, whereas stress components have a physical unit, e.g., pascals. Therefore, the absolute stress values cannot be determined only from orientations. Instead, the principal stress axes and stress ratio are inferred. The ratio is defined as $\Phi = (\sigma_2 - \sigma_3)/(\sigma_1 - \sigma_3)$ (Bishop, 1966), where σ_1, σ_2 and σ_3 are the principal stresses
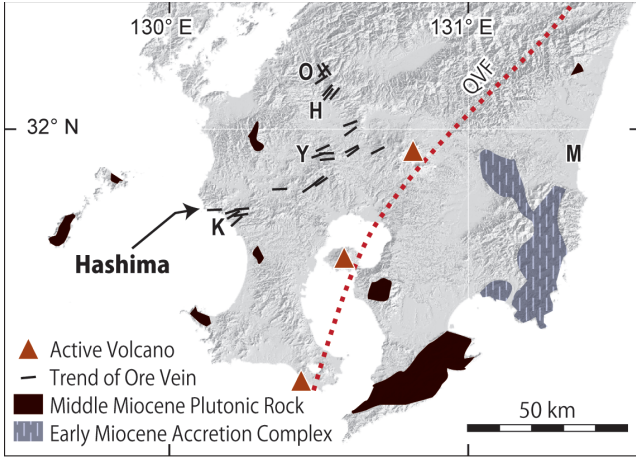
Figure 1: Trends of ore veins in southern Kyushu, Japan, after Izawa (2004). Geological map of southern Kyushu simplified from Geological Survey of Japan (1992). H, Hishikari; K, Kushikino; M, Miyazaki; O, Okuchi; QVF, Quaternary volcanic front; Y, Yamagano.
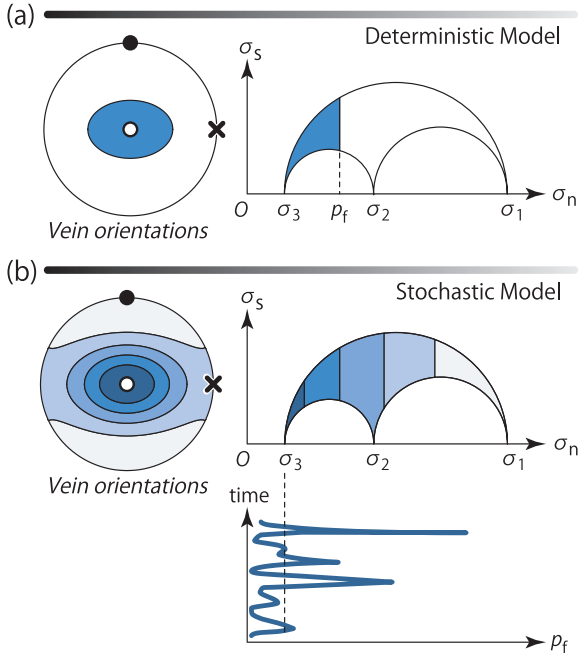

Figure 2: Schematic illustrations showing the model of Baer et al. (1994) and Jolly and Sanderson (1997) (a), and our model (b) for the formation of epithermal veins. Equal-area projections show the poles to veins; closed circle, cross and solid circle indicate σ_1, σ_2 and σ_3 orientations, respectively. The former model assumes that vein minerals were deposited from thermal fluid with a distinctive pressure, p_f. Veins are thought to be formed in fractures with its normal stress, σ_n, being smaller than p_f, when p_f is greater than σ_3. As a result, the poles to veins are confined in an elliptical cone or along a girdle in the deterministic model. In contrast, the we assume fluctuating fluid pressure. The poles are thought to show a nebulous pattern on the stereogram in our model due to fluctuating p_f: gradation in the stereogram and the Mohr diagram depict the number density of data points.
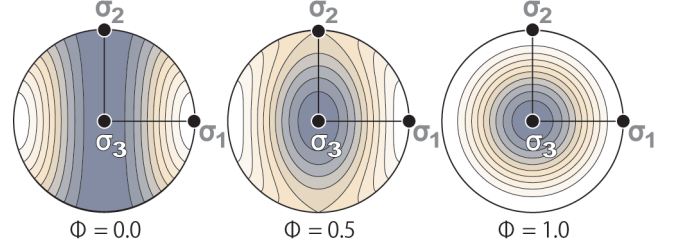

Figure 3: Equal-area projections showing the contours of σ_n for three Φ values. Planes perpendicular to the σ_3- and σ_1-axes have the minimum and maximum σ_n values. With the increase of Φ from 0 to 1, the region of the least σ_n values changes its shape from a girdle through an ellipse to a circle.

($\sigma_1 \geq \sigma_2 \geq \sigma_3$), and compression is positive in sign. Pressure of the fluid, from which veins were formed, is normalized through the equation, $p = (p_f - \sigma_3)/(\sigma_1 - \sigma_3)$. This is identical with the "normalized driving pressure" of Baer et al. (1994).

In this article, we use the term "a state of stress" to refer to the stresses collectively that have the principal orientations and stress ratios in common. As the absolute values are not evaluated in this work, we identify the principal stresses as $\sigma_3 = 0$, $\sigma_2 = \Phi$ and $\sigma_1 = 1$. Accordingly, stress tensor has the form, $\boldsymbol{\sigma} = \mathbf{E}^\top \boldsymbol{\sigma}_0 \mathbf{E}$, where

$$\boldsymbol{\sigma}_0 = \begin{pmatrix} 1 & 0 & 0 \\ 0 & \Phi & 0 \\ 0 & 0 & 0 \end{pmatrix} \tag{1}$$

is the simplest 3×3 matrix to have the information of Φ, and $\mathbf{E}$ is the orthogonal matrix representing the principal orientations. A fracture surface with the unit normal, $\mathbf{v}$, is subject to the traction, $\mathbf{t} = \boldsymbol{\sigma}\mathbf{v}$, which has the normal and shear components,

$$\sigma_n = \mathbf{v}^\top \mathbf{t} = \mathbf{v}^\top \mathbf{E}^\top \boldsymbol{\sigma}_0 \mathbf{E} \mathbf{v} \tag{2}$$

$$\sigma_s = |\mathbf{t} - \sigma_n \mathbf{v}|, \tag{3}$$

in the ranges $0 \leq \sigma_n \leq 1$ and $0 \leq \sigma_s \leq 1/2$ (Table 1). Equal-area projections in Fig. 3 show the correspondence between σ_n and $\mathbf{v}$ for three Φ values.

2.2. Basic assumptions

To determine the state of stress from a nebulous pattern of poles to veins, some rule relating vein orientations to stress is necessary. We have the four assumptions for the formation of a cluster of veins:

1. The state of far field stress did not change during the formation of the cluster.

2. The country rock was effectively isotropic for the vein orientations to inherit orthorhombic symmetry from the stress (Baer et al., 1994) (Fig. 3).

3. Veins were formed on fracture surfaces only if the normal stresses acting on them were smaller than the pressure of thermal fluid from which vein minerals were precipitated (Delaney et al., 1986) (Fig. 2).

4. The cluster was formed as a result of multiple ascending events of thermal fluids with various fluid pressures.

Table 1: List of symbols used in this article. All vectors are expressed by column matrices.

A	normalization constant of the Bingham distribution
$\mathbf{E}$	orthogonal matrix denoting the symmetry axes of σ or of the Bingham distribution
$\mathbf{e}^{(1)}, \mathbf{e}^{(2)}, \mathbf{e}^{(3)}$	unit vectors denoting symmetry axes of σ or of the Bingham distribution
N	number of veins
N_b	number of bootstrap sample sets
$\mathcal{P}(\ )$	probability distribution function
p	normalized fluid pressure
p^*	lower bound of the maximum p
p_f	fluid pressure
$\top$	matrix transpose
$\mathbf{v}$	unit vector perpendicular to a vein
$\mathbf{v}^{(i)}$	unit vector perpendicular to the ith vein
$\mathbf{x}$	5-dimensional unit vector representing a state of stress
$\bar{\mathbf{x}}$	5-dimensional unit vector representing the state of stress optimal for data
Θ	distance between stress states
$\overline{\Theta}$	uncertainty of the optimal state of stress
κ_1, κ_2	concentration parameters of the Bingham distribution
Λ	measure of how often veins are formed on fractures subject to high normal stresses
Φ	stress ratio or normalized intermediate principal stress
σ	stress tensor normalized to have the principal stresses, 0, Φ and 1
$\sigma_1, \sigma_2, \sigma_3$	principal stresses
$\sigma_\mathrm{n}, \sigma_\mathrm{s}$	normal and shear stresses
ς	reduced stress tensor normalized by its first and second basic invariants

The first assumption is essential—it is beyond the scope of this study to deal with heterogeneous data. Geological media are heterogeneous and anisotropic to some extent. The second assumption, i.e., the effective isotropy, means that the internal structures of the host rock, e.g., bedding planes, sedimentary particles and their matrix and pre-existing fractures, are thought to have negligible effect in a statistical sense for vein orientations as a whole. We do not consider the reason for the attitude of each fracture. The network and interaction of fractures (e.g., Blenkinsop, 2008) are neglected in this work: Baer et al. (1994) considered their effects. As a result, number density of the poles to veins is expected to have contours along those of σ_n on a stereogram (Fig. 3), if the number of veins is large. The third assumption leads us to exclude data from veins formed in shear fractures, which can give rise to the deposition of minerals, e.g., slickenfibers, irrelevant to the present problem.

There are lines of evidence for the fourth assumption. A cluster of epithermal veins has variations in their lithology and in formation temperature to some extent (e.g., Izawa et al., 1981; Sanematsu et al., 2006). In the Hishikari ore field (Fig. 1), a thick vein grew in distinct episodes separated by 30 to 110 kyr (Sanematsu et al., 2006); and the economically most important mineralization lasted only for ~50 kyr, while mineralization in the field lasted for ~300 kyr (Sekine et al., 2002). Sibson (1987) argued that such episodic movements of thermal fluids are linked with earthquake swarms. Economically important swarms often have such veins that include breccias brought from host rocks by thermal fluid rushing up in fractures. But,

not all veins of a swarm contain breccias. Thermal fluids had various impetuses.

From the third assumption, the fractures in which veins were formed in an event had normal stresses satisfying the condition $0 < \sigma_\mathrm{n} < p$, where p is the fluid pressure of the event. Thanks to the orthorhombic symmetry of stress tensors, it is enough to consider a quadrant of the principal stress coordinate system. Fig. 4 is the schematic illustration showing the formation of a vein cluster by the episodic mineralization with the non-dimensional fluid pressures at 0.2, 0.4, 0.1 and so on. Thermal fluids have to permeate fractures before they deposit minerals, while fracture permeability decreases with increasing σ_n on the fractures (e.g., Pyrak-Nolte and Morris, 2000; Uehara and Shimamoto, 2008). Hence, normal stresses on the fractures in which veins were formed in an event have a frequency distribution denoted by a decreasing function of σ_n with the ceiling at the p value of the event.

Episodic mineralization could have had different fluid pressures. We consider that low p fluids passed through the observed rock mass more often than high p fluids. Veins we observe today are the result of those events. Low σ_n fractures had chances to be mineralized more often than high σ_n ones. Consequently, the probability distribution of vein orientations can be expressed by a decreasing function $f(\sigma_\mathrm{n})$ from the σ_3- to σ_1-orientations (Fig. 3). That is, Eq. (2) leads to the expression,

$$\mathcal{P}(\mathbf{v}) \propto f(\mathbf{v}^\top \mathbf{E}^\top \sigma_0 \mathbf{E} \mathbf{v}), \qquad (4)$$

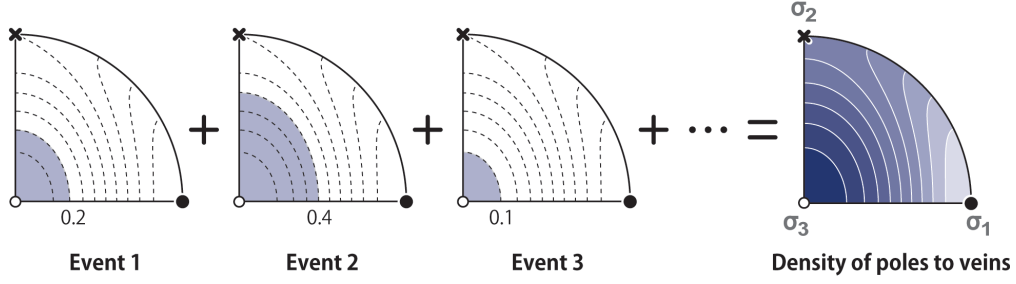for the frequency of veins perpendicular to $\mathbf{v}$.

3

Figure 4: Schematic picture for the formation of a cluster of veins under a state of stress with $\Phi = 0.6$. Each fan shows a quadrant of the equal-area projection: open circle, cross and closed circle indicate the σ_1-, σ_2- and σ_3-orientations, respectively. Colored area in the quadrant illustrates the fractures in which veins can be formed. Dotted lines indicate the contours of σ_n with the intervals of 0.1. Event 1 is assumed to have resulted in the first group of veins from a fluid with $p = 0.2$, by which poles to the veins are enveloped by the contour of $\sigma_n = 0.2$. The succeeding events are assumed to have had the pressures at 0.4, 0.1, and so on. In addition, we assume that low p fluids came up more often than high p ones. As a result, orientations of the veins that we observe today have the maximum and minimum densities at the σ_3- and σ_1-orientations, respectively. And, the orientation distribution has contours (white lines) along iso-σ_n lines on the equal-area projection.

2.3. Bingham distribution

The form of the function $f(\sigma_n)$ is not well known. For mathematical simplicity, we hypothesize an exponentially decreasing function,

$$\mathcal{P}(\mathbf{v}) \propto \exp\left(-\mathbf{v}^\top \mathbf{E}^\top \sigma_0 \mathbf{E}\mathbf{v}/\Lambda\right), \tag{5}$$

where Λ is a constant standing for the frequency of high p fluids passing through the rock mass compared to low p ones. The orientation distribution denoted by Eq. (5) is known as the Bingham distribution, and here, relates the nebulous pattern of vein orientations to a stress state. The choice of the exponential function is arbitrary—a discussion of this is given in §5.1.

The Bingham distribution is the well understood and it is the simplest extension of the multivariate normal distribution to the orientation distribution with orthorhombic symmetry (Bingham, 1974). The distribution has the probability density,

$$\mathcal{P}_{\mathrm{B}}(\mathbf{v}) = \frac{1}{A} \exp\left(\mathbf{v}^\top \mathbf{E}^\top \mathbf{K}\mathbf{E}\mathbf{v}\right), \tag{6}$$

where A is the normalization constant, and

$$\mathbf{K} = \begin{pmatrix} \kappa_1 & 0 & 0 \\ 0 & \kappa_2 & 0 \\ 0 & 0 & 0 \end{pmatrix} \tag{7}$$

is the matrix characterizing the distribution (Love, 2007). In this case, $\mathbf{E}$ is the orthogonal matrix representing the axes of the minimum, intermediate and maximum concentrations, respectively. The parameters, κ_1 and κ_2, are negative in sign, and their absolute values denote concentrations. The spread of orientations from the maximum to minimum concentration axes is denoted by $1/|\kappa_1|$, and that from the maximum to intermediate concentration axes is denoted by $1/|\kappa_2|$ (Fig. 5).

Comparing the Bingham distributions denoted by Eqs. (5) and (6), we obtain

$$-\frac{1}{\Lambda}\begin{pmatrix} 1 & 0 \\ 0 & \Phi \end{pmatrix} = \begin{pmatrix} \kappa_1 & 0 \\ 0 & \kappa_2 \end{pmatrix}. \tag{8}$$

in terms of Eqs. (1) and (7). It follows that Φ and Λ satisfy
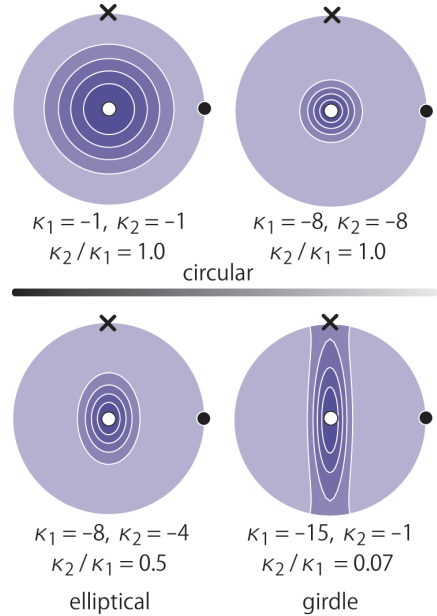
$$\Phi = \kappa_2/\kappa_1 \tag{9}$$

Figure 5: Equal-area projections of the Bingham distributions for several κ_1 and κ_2 values. Solid and open circles indicate the axes of the maximum and minimum concentrations, respectively. The intermediate concentration axis perpendicular to them is indicated by crosses.

and $\Lambda = -1/\kappa_1$. The comparison leads to the correspondence of the σ_1-, σ_2- and σ_3-axes with the maximum, intermediate and minimum concentration axes, respectively.

3. Paleostress analysis

3.1. Optimal solution

The state of stress optimal for a cluster of veins is obtained from the Bingham distribution that best fits the vein orientations. We employed the maximum likelihood estimator (e.g., van den Bos, 2007) for this optimization. That is, $\mathbf{E}$ and $\mathbf{K}$ are

optimized by maximizing the logarithmic likelihood function,

$$\mathcal{L}(\mathbf{E}, \mathbf{K}) = \sum_{i=1}^{N} \log \mathcal{P}_B(\mathbf{v}^{(i)}, \mathbf{E}, \mathbf{K}), \qquad (10)$$

where $\mathbf{v}^{(i)}$ is the unit normal of the ith vein, and N is the number of veins. Combining Eqs. (6) and (10) we have

$$\mathcal{L}(\mathbf{E}, \mathbf{K}) = \sum_{i=1}^{N} \left[\mathbf{v}^{(i)}\right]^{\top} \mathbf{E}^{\top} \mathbf{K} \mathbf{E} \mathbf{v}^{(i)} - N \log A. \qquad (11)$$

A is a function of $\mathbf{K}$, and was evaluated by the numerical integration of the probability density over the unit sphere (Tanaka, 1999). We began the maximization from the initial condition, $\kappa_1 = \kappa_2 = -10$; $\mathbf{E}$ was initialized using the eigenvectors of the orientation matrix (Borradaile, 2003) of the vein orientations,

$$\mathbf{v}^{(1)}[\mathbf{v}^{(1)}]^{\top} + \cdots + \mathbf{v}^{(N)}[\mathbf{v}^{(N)}]^{\top}. \qquad (12)$$

Once $\mathbf{E}$ and $\mathbf{K}$ were optimized for the data, the optimal stress ratio, $\hat{\Phi}$, was evaluated via Eq. (9).

We envisage that overpressured fluids episodically left veins. The fluids are assumed to have had different pressure values. The normal stresses that acted on the vein walls were capped by the maximum pressure of the fluids (Fig. 4). On one hand, the quantity

$$p^* = \max\left(\hat{\sigma}_n^{(1)}, \ldots, \hat{\sigma}_n^{(N)}\right) \qquad (13)$$

can be calculated from the data, where $\hat{\sigma}_n^{(i)}$ ($i = 1, \ldots, N$) is the normal stress on the ith vein evaluated using the optimal stress and Eq. (2). On the other hand, we cannot expect to observe the particular veins that were formed from the fluid with the maximum pressure because a vein cluster always includes unobserved members. It is difficult to estimate the maximum pressure, but p^* is the lower bound of the maximum.

3.2. Error analysis

The confidence regions of the optimal stress axes and stress ratio were estimated by the bootstrap method. That is, the N data were resampled N_b times with repetition ($N_b \gg N$). And, we obtained N_b stress states as the optimal solutions from the N_b data sets. Uncertainty of the optimal solution was evaluated from them through the following procedure.

1. The stress states were transformed to 5-dimensional unit vectors, $\mathbf{x}^{(1)}, \ldots, \mathbf{x}^{(N_b)}$ (Appendix A).
2. A unit vector is computed as the mean of the unit vectors:

$$\overline{\mathbf{x}} = [\mathbf{x}^{(1)} + \cdots + \mathbf{x}^{(N_b)}]/|\mathbf{x}^{(1)} + \cdots + \mathbf{x}^{(N_b)}|.$$

   The uncertainty of the optimal stress was denoted by the spread of the unit vectors around $\overline{\mathbf{x}}$ (Yamaji and Sato, 2006).
3. Distances of the unit vectors from $\overline{\mathbf{x}}$ were computed via Eq. (A.4) to evaluate the spread. Let $\Theta^{(i)}$ be the distance between $\mathbf{x}^{(i)}$ and $\overline{\mathbf{x}}$.
4. The N_b unit vectors were sorted by their Θ vales in ascending order.

5. The 95% confidence region of the optimal stress state was represented by the spread of the unit vectors excluding 5% of the vectors that were the most distant from $\overline{\mathbf{x}}$. Thus, the last 5% of the unit vectors were excluded from the following processing. Let n be the maximum integer satisfying $n \le 0.95 N_b$.
6. The remaining n unit vectors were converted to the corresponding reduced stress states through Eq. (A.3).
7. Finally, the 95% confidence regions of the optimal stress state were obtained as the envelopes of the n stress axes on a stereogram and of the n values of Φ on a histogram.

In addition to the confidence regions, it is sometimes convenient to use a single precision parameter. To this end, we adopt the "mean angular stress distance" (Yamaji and Sato, 2006): $\overline{\Theta} = [\Theta^{(1)} + \cdots + \Theta^{(N_b)}]/N_b$. If the N_b stress states are completely random, $\overline{\Theta}$ has the maximum value of 90°, meaning that stress is not constrained at all from data. If all the stress states are identical, we have $\overline{\Theta} = 0°$. Precisely determined stress states have small $\overline{\Theta}$ values.

4. Application to the Hashima data

4.1. Geologic setting

A cluster of veins occurs on the coast of Hashima village (Fig. 6), western part of the Kushikino metallogenic district, southern Kyushu (Fig. 1). Kushikino deposits were formed at the paleo temperatures of 210–250°C and at the depths of 450–850 m (Izawa et al., 1981). Adularia and illite from a vein of the cluster yielded the K-Ar ages of 3.55 ± 0.11 and 3.67 ± 0.09 Ma, respectively (Izawa and Zeng, 2001). The veins are hosted by massive, altered tuff breccia of the Hokusatsu Koki Andesites, which yielded the K-Ar ages of 4.0–4.2 Ma (Ministry of International Trace and Industry, 1979; Izawa and Zeng, 2001). The host rock is composed of poorly sorted matrix including granule to pebble sized breccias. Bedding surfaces were sporadically observed with a westward dip of $\lesssim 15°$, gentle enough for us not to consider tilt-correction of the data. Cretaceous and older accretionary complexes make up the basement of the Andesites. A Jurassic complex was found at the depth of 140 m below sea-level near the village (Morishita and Teraoka, 1996).

Until the extrusion of the Hokusatsu Koki Andesites, southern Kyushu situated in the fore-arc, except for the short-term unusual fore-arc magmatism in the early Middle Miocene (e.g., Yamaji and Yoshida, 1998). The volcanic front migrated oceanward (eastward) during the Pliocene in southern Kyushu (Izawa and Watanabe, 2001), probably indicating slab rollback under Kyushu (Yamaji, 2003).

4.2. Data acquisition

We observed quartz veins on the wave-cut platform in front of Hashima village (Fig. 6a). Their attitudes were measured at 233 points in a 100 m × 200 m area. The veins have variations to some extent in lithology and thickness, but we deal with their orientations equally in this work. The thickness ranged from 1 mm to 300 mm, but those thinner than 50 mm were dominant.
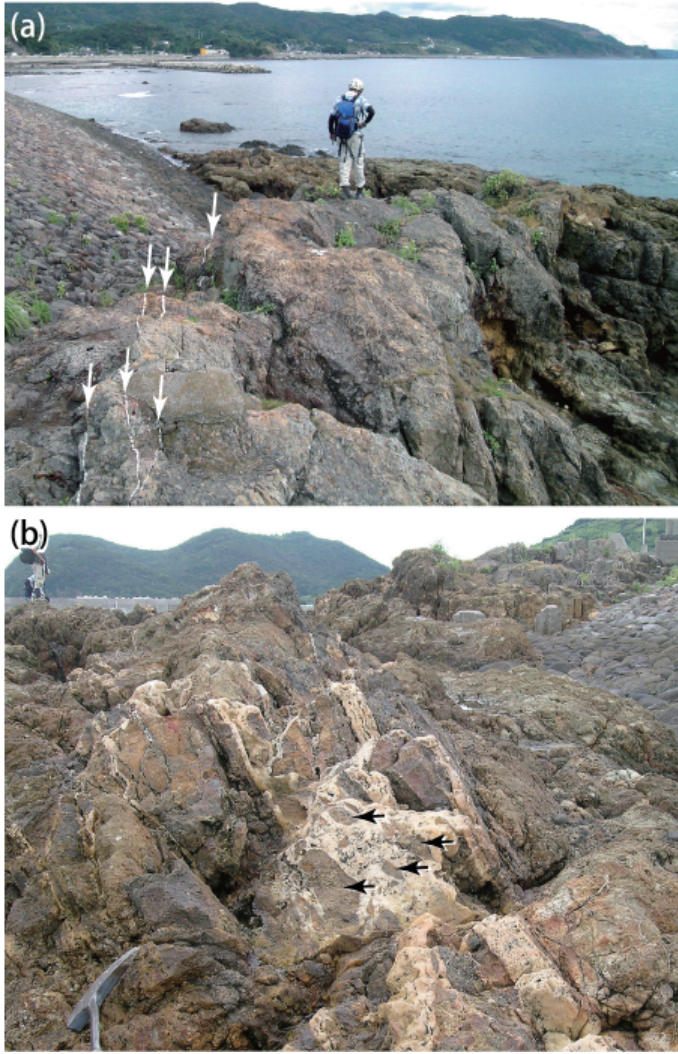
Figure 6: (a) Photograph showing quartz veins (arrows) cropping out at the Hashima site. A person for the scale of surface undulations of the wave-cut platform in front of Hashima village. (b) Thick quartz vein including breccia (arrows).
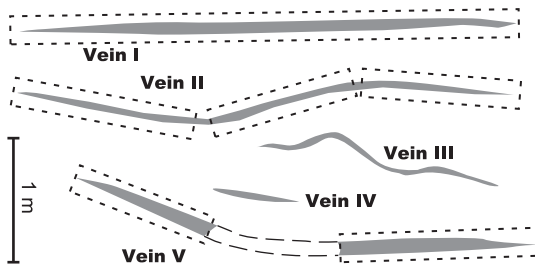

Figure 7: Schematic illustration showing the method of data acquisition using a threshold length of 1 meter. Vein I is a planar vein, and its general trend is shown by dotted line. Vein II has bends. In this case, the planar portions with their traces on the outcrop are longer than 1 meter are used to approximate this vein, and the attitudes of the portions are measured as independent data. Veins III and IV have no segment longer than 1 meter. So, they are ignored. Vein V has the bend that is not exposed, but has planar segments longer than 1 meter. In this case, the planar portions are measured.

We saw 9 veins including breccias from the host rock (Fig. 6b), and one from older quartz veins, suggesting the rapid passage of thermal fluids capable of transporting the breccias. Veins generally had rough surfaces. Only one vein had slickenside on its upper wall, which we excluded from data for paleostress analysis. Other veins had neither slickenfiber lineations nor slickensides. The rough surfaces and the absence of sheared structures suggest that most of the Hashima veins were formed in mode I or mixed-mode cracks.

It is straightforward to measure a vein orientation, if the vein is planar and its entire length is exposed. Vein I in Fig. 7 illustrates such an ideal case. Veins II through V in this figure show other cases. There were curved veins with the radius of curvature of the order of 10^{-1}–10^{0} m like Vein II. The trace of such a vein on the outcrop was approximated by straight line segments, each of which was longer than 1 m; and the attitude of the vein was measured on each segment. This threshold was chosen to deal with veins much larger than the breccias in the host rock for diminishing the effect of the heterogeneity coming from the breccias and their matrix. Short segments and sharp bends like Veins III and IV were neglected. Long, curved ones yielded two or more data. We chose such a treatment to cope with the lack of exposure. For example, Vein V in Fig. 7 has a bend at its center, but the central part is obliterated. We do not know whether one or two veins exist in this case. So, we measured the attitudes of both the planar ends. For equal treatment of veins with good and poor exposures, we measured the attitudes on the wide planar parts of veins. As a result, there were 20 veins, each of which provided two or three orientation data. We saw dozens of veins with offshoots, from which we obtained orientation data if they met the criteria. Stowell et al. (1999) documented that quartz veins in North Wales had offshoots consistently oriented anticlockwise from main veins. We saw no such systematic relationship between main veins and their offshoots.

4.3. Result

The stereoplot in Fig. 8 shows attitudes of the Hashima veins. Surface undulations of the wave-cut platform with an amplitude of a few meters (Fig. 6) gave us the opportunity to observe horizontal or low-dipping veins, but there were none. Therefore, it is impossible to attribute their absence to sampling bias. Poles to the veins were distributed along a subhorizontal girdle, and had the maximum concentration at the trend of 150–180°. The orientation of the minimum concentration along the girdle makes more or less a right angle with this trend. Consequently, the orientation distribution had a roughly orthorhombic symmetry.

The state of stress determined from the Hashima data is shown in Fig. 8 and Table 2. We obtained a normal-faulting regime of stress with the optimal stress ratio of ~0.2. The lower bound of the maximum fluid pressure (Eq. 13) was $p^* = 0.55$. It is clear from the histogram in Fig. 9 that most of the vein minerals were precipitated on the fractures with $\hat{\sigma}_n$ smaller than 0.2–0.3.

The bootstrap method resulted in the uncertainty of $\overline{\Theta} = 4.28°$: the solution was so precisely determined that if faults
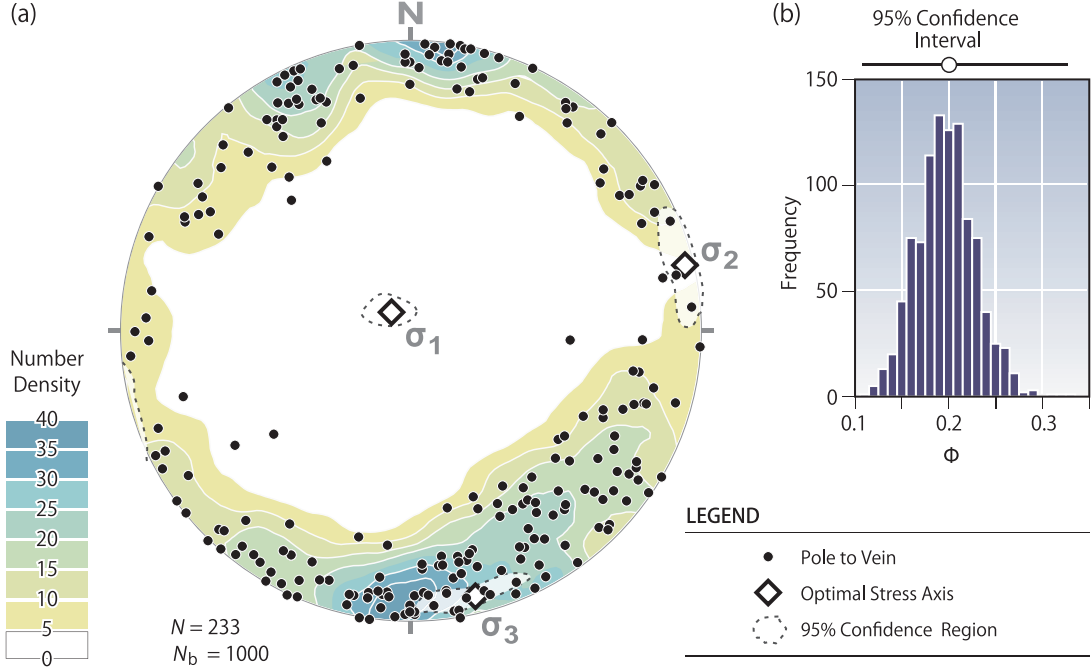
Figure 8: Hashima data and the result of the present method applied to them. (a) Lower-hemisphere, equal-area projection. Contours indicate the number of poles per 0.1 steradians, corresponding to the number of poles within a small circle with the radius of ~10°. (b) Histogram showing the frequency distribution of the stress ratios evaluated from the data by the bootstrap method. Open circle depicts the optimal Φ value.

Table 2: The state of stress optimal for the Hashima data and its 95% confidence limit.

	Trend	Plunge
σ_1-axis	314° +57°/−43°	82° +5°/−6°
σ_2-axis	076° +13°/−11°	4° ± 6°
σ_3-axis	167° ± 13°	7° ± 4°
Φ	0.20 +0.13/−0.09	
κ_1	−7.9 +1.8/−2.5	
κ_2	−1.6 +0.5/−0.9	
$\overline{\Theta}$	4.28°	

are activated by the optimal stress, their slip directions can be predicted with this level of uncertainty (Yamaji and Sato, 2006). This solution has the σ_3-axis in the region that has the largest orientation density, and the σ_2-axis at around the least density on the girdle. The confidence region of the optimal solution is illustrated in Fig. 8. The σ_1-axis was determined more precisely than the remaining stress axes, the confidence regions of which were elongated along the girdle.

4.4. Robustness of the solution

The present method is not only capable of determining stresses from veins with nebulous pole orientations, but also works well with data sets from a limited number of veins. To show this benefit, the method was applied to subsets with various sizes taken from the Hashima data. That is, m-element subsets were randomly sampled from the Hashima data, where
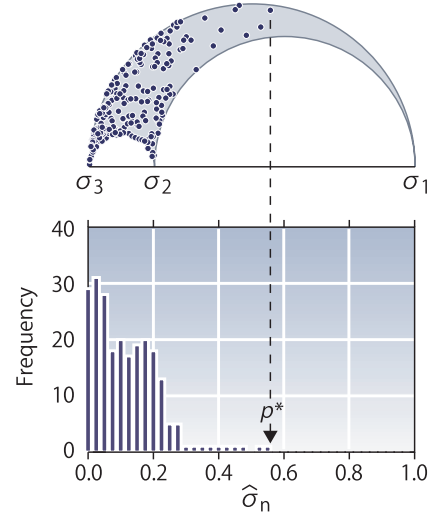

Figure 9: Mohr diagram and histogram of $\hat{\sigma}_n$, i.e., non-dimensional normal stresses on Hashima veins evaluated in terms of the optimal stress state (Fig. 8). Thermal fluids with various pressures passed fractures of the host rock, and p^* indicates the lower bound of the maximum pressure of the fluids.
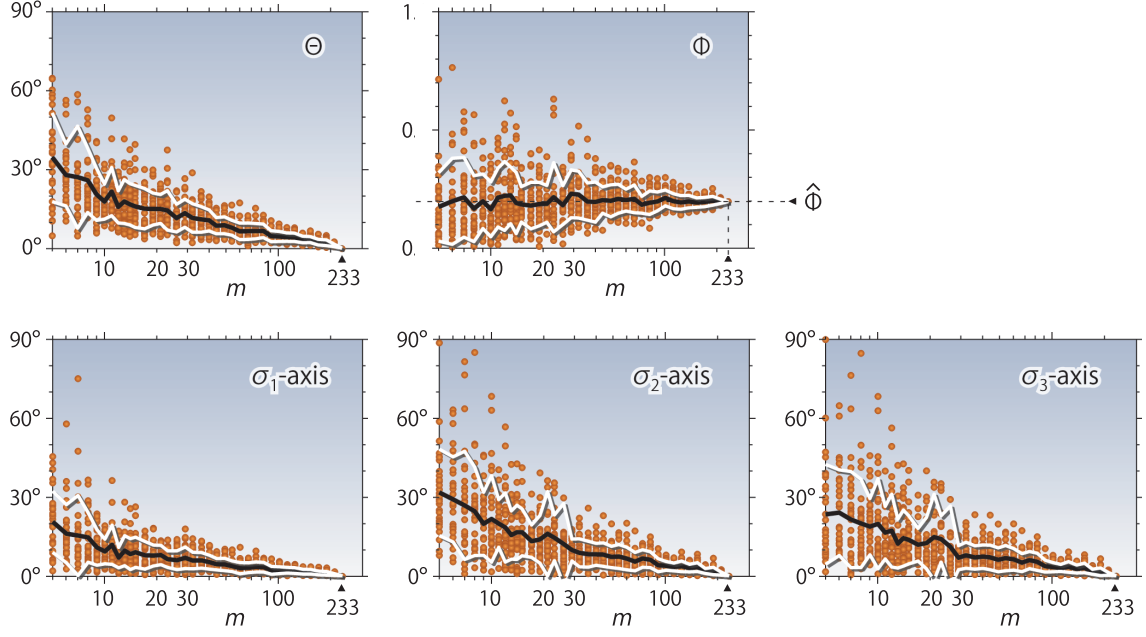
7

Figure 10: Semi-log plots showing convergence of the differences between the solutions determined from m-element subsets of the Hashima data and the optimal solution determined from the entire Hashima data with increasing m toward $N = 233$. Θ is the distance between the stress states represented by the solutions (Appendix A). $\hat{\Phi}$ is the optimal stress ratio for the entire data. Ordinates of the lower three diagrams indicate the angles between the stress axes of the solutions. Solid lines depict the mean differences for the 30 subsets with the same number of elements. While lines indicate their standard deviations. The convergence at $m = 20$–30 indicates that the minimum size of data is 20–30 for the Hashima veins to conduct our stress inversion, and that the optimal solution from the 233 data was numerically stable.

m is greater than 5. Thirty subsets were generated as such for each m value; the results of the present method applied to the subsets were compared with the optimal solution obtained from the entire Hashima data.

It was found that the solutions became unstable for $m \lesssim 20$. That is, the Θ distance between the solution of a subset and the optimal solution gradually increased with the decreasing m, and showed spikes for $m \lesssim 20$ (Fig. 10). The σ_1-axis were more precisely determined than the other axes, because Φ had relatively low values. If the permissible error is ~30° for the angles between the stress axes of the optimal solution and those determined from the subsets, at least ~30 data were necessary to estimate the state of stress for the case of Hashima veins. For subsets with m greater than ~20, the method robustly worked, and yielded similar solutions. But, generally, the least number of data for the method to work depends on data.

4.5. Comparison with the Jolly-Sanderson method

The method of Jolly and Sanderson (1997) was applied to the Hashima data for comparing results. Fig. 11 shows the vein orientations relative to the stress axes that were determined as the eigenvectors of the orientation matrix of the veins (Eq. 12). The eigenvectors largely coincided with our optimal stress axes: the difference was less than 1°. The method evaluates stress ratio and normalized driving pressure by the formulas, $\Phi = 1 - (1 - \cos 2\theta_2)/(1 - \cos 2\theta_3)$ and $p = (1 + \cos 2\theta_2)/2$, respectively (Eqs. 16 and 17 of Jolly and Sanderson, 1997), where θ_2 and θ_3 are the minimum and maximum apertures of the elliptical cone that excludes most of the poles. The cones

with the apertures, $\theta_2 = 56°$ and $\theta_3 = 80°$, in Fig. 11a were drawn to have a orthorhombic symmetry by eye. The solid circle in Fig. 11b shows the corresponding Φ value at 0.3. The nebulous pattern made by the data points led to the ranges of possible θ_2 and θ_3 angles depicted by a stippled region in this subfigure. The region was chosen on the stereogram by eye. Our 95% confidence interval included the possible Φ values denoted by this region.

Jolly and Sanderson (1997) assumed that a fluid with the pressure R' dilated fractures to form veins, but we assume that fluids with various pressures did so. Therefore, our model does not have a quantity corresponding to p. However, the possible range of p between 0.22 and 0.36 (Fig. 11b) coincided roughly with the rapid decline in the histogram of $\hat{\sigma}_n$ in Fig. 9.

5. Discussion

5.1. Methodology

In order to relate the Bingham distribution (Eq. 5) to a stress state, the exponential function was used in this work as the decreasing function of Eq. (4) for mathematical simplicity. That is, taking the logarithm eliminates the exponential function in the likelihood function to make the object function of the optimization problem very easy such that Eq. (10) was reduced to Eq. (11). Unfortunately, the exact forms of the probability distribution of σ_n and v are not known, and the choice of the exponential family of probability distributions is arbitrary.

However, the state of stress determined from vein orientations is not sensitive to the choice of the probability distribution

8

of σ_n as long as it is a decreasing function. The distribution of σ_n values on a stereogram is completely determined by stress axes and Φ (Fig. 3). Contour lines of $\mathcal{P}(\sigma_n)$ on a stereogram coincide with those of σ_n values, as long as σ_n has a one-to-one correspondence with $\mathcal{P}(\sigma_n)$ (§2.2). Power-law distributions can be alternatives to our exponential distribution, because vein widths and lengths are known to show such distributions (e.g., Roberts et al., 1999; Bonnet et al., 2001). However, both the exponential and power-law distributions are so flexible that they can approximate each other (Fig. 12). Therefore, the choice from those distributions is peripheral to determine the optimal stress state for vein orientations.

The orientation distribution of the Hashima veins was consistent with the Bingham distribution. However, the Bingham hypothesis should be challenged in future, like the Wallace-Bott hypothesis, which is essential for the stress inversion of faults and seismic focal mechanisms, was repeatedly challenged by researchers (e.g., Dupin et al., 1993; Pollard et al., 1993; Pascal, 2002). The effect of interaction among fractures is also a subject of further study for paleostress analysis using vein orientations.

Recently, the absolute values of fluid pressures (p_f) were crudely estimated from the width-length ratios of clustered veins (Gudmundsson, 1999; Mazzarini and Isola, 2007), where the host rocks were assumed to be linear elastic bodies, and possible values of Poisson ratio and Young's modulus were assumed for estimating the absolute values. The combination of the technique of evaluating representative p_f and our stochastic modeling shall improve our understanding of fluid migration in the crust.

The present method is based on the hypothesis that poles to veins obey the Bingham distribution. Jolly and Sanderson (1997) used the distribution as well to determine stress axes. The Jolly-Sanderson method resulted in the possible range of Φ from the Hashima data similar to our 95% confidence interval, but the uncertainty of Φ estimated by eye on the stereogram in Fig. 11a inevitably includes subjectivity.

5.2. Tectonic implications

From the Hashima veins we obtained a normal faulting regime of stress. That is, the σ_2- and σ_3-axes were more or less horizontal, when the veins were formed. In addition, we obtained a relatively low stress ratio, indicating a small horizontal differential stress, $\sigma_2 - \sigma_3$. This means that σ_2- and σ_3-axes could have been easily rotated by perturbations from, e.g., magmatic and topographic loading (e.g., Mogi, 1958; Kervyn et al., 2008).

Not only horizontal but also the full differential stress, $\sigma_1 - \sigma_3$, was small as well. This is evidenced by the very rare occurrence of sheared meso-structures. Some of the veins had jigsaw-fitting walls, but they did not indicate displacements along veins. Slickenlines and slickenfibers were not found except for a wall of a vein in the study field. Since the Hashima veins have various attitudes, a large differential stress should have resulted in shear fracturing especially along fractures oblique to stress axes. The low stress level suggested by the Hashima veins is consistent with the model of the formation
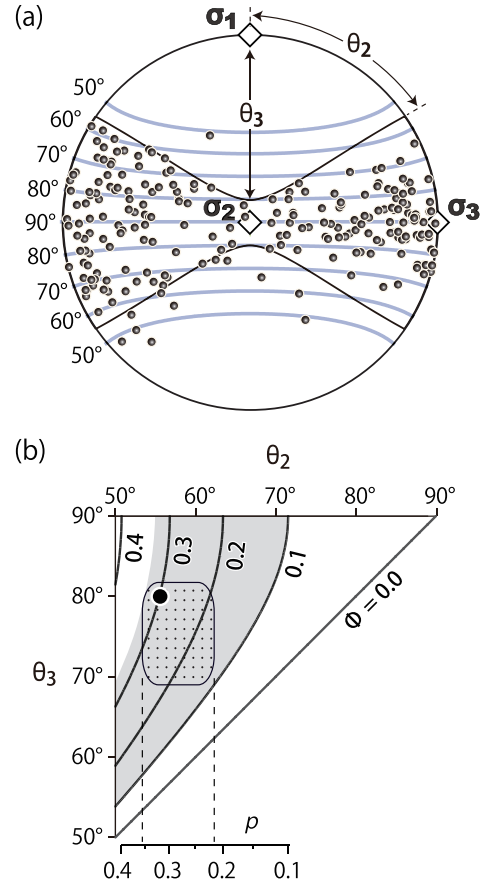

Figure 11: (a) Equal-area projection of the Hashima data for the method of Jolly and Sanderson (1997). Diamonds show the stress axes determined as the eigenvectors of the orientation matrix of the vein orientations. Solid lines roughly envelope the data points. Parallels centered by the σ_1-axis are drawn to measure θ_2 and θ_3. (b) Stress ratio (thick line) and fluid pressure (p) estimated from the Hashima data by the Jolly-Sanderson method. Solid circle indicates those estimates corresponding to the solid lines in (a). Stippled region indicates possible ranges of the angles. Gray region depicts the 95% confidence interval of Φ evaluated by the present method.
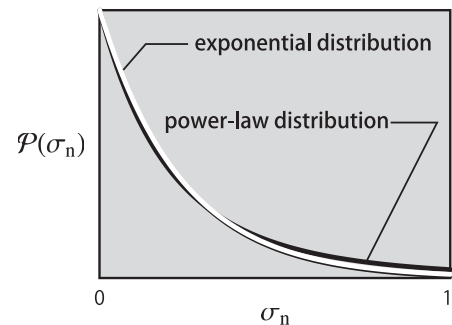

Figure 12: Graphs showing the exponential and power-law distributions that have approximately equal values.

of epithermal veins by Sibson (1996, p. 1040). That is, epithermal veins were formed from a large volume of thermal fluid under a low differential stress at a shallow depths (< 1 km).

Appendix A. Distance between stress states

To evaluate the uncertainty of the optimal solution, distance between stress states have to be properly defined. The stress tensor, σ, used in §2 was normalized to have the eigenvalues at 0, Φ and 1. In order to define distance between stress states, we introduce another stress tensor, which was originally proposed for fault-slip analysis. That is, we make use of the formulation of Sato and Yamaji (2006): a reduced stress tensor is denoted by a 3×3 matrix of the form,

$$\boldsymbol{\varsigma} = \mathbf{E}^\top \left[\frac{\text{diag}(2 - \Phi, 2\Phi - 1, -\Phi - 1)}{\sqrt{3\Phi^2 - 3\Phi + 3}} \right] \mathbf{E}, \qquad (A.1)$$

where $\mathbf{E}$ is the orthogonal matrix representing the principal axes. $\boldsymbol{\varsigma}$ is normalized so as to have the first and second basic invariants being equal to 0 and 1, respectively.

Let ς_{ij} be the ijth component of $\boldsymbol{\varsigma}$. Then, a one-to-one correspondence exists between $\boldsymbol{\varsigma}$ and a 5-dimensional unit vector $\mathbf{x}$, the components of which are

$$
\begin{aligned}
x_1 &= -\left(\frac{\sqrt{2}}{4} + \frac{\sqrt{6}}{12} \right) \varsigma_{11} + \left(\frac{\sqrt{2}}{4} - \frac{\sqrt{6}}{12} \right) \varsigma_{22} + \frac{1}{\sqrt{6}} \varsigma_{33} \\
x_2 &= \left(\frac{\sqrt{2}}{4} - \frac{\sqrt{6}}{12} \right) \varsigma_{11} - \left(\frac{\sqrt{2}}{4} + \frac{\sqrt{6}}{12} \right) \varsigma_{22} + \frac{1}{\sqrt{6}} \varsigma_{33} \\
x_3 &= \varsigma_{23} \\
x_4 &= \varsigma_{31} \\
x_5 &= \varsigma_{12}.
\end{aligned}
\qquad (A.2)
$$

Therefore, we identify $\mathbf{x}$ with a state of stress. On the other hand, given $\mathbf{x}$, the corresponding reduced stress tensor can be obtained through the equations,

$$
\begin{aligned}
\varsigma_{11} &= -\left(\frac{1}{\sqrt{2}} + \frac{1}{\sqrt{6}} \right) x_1 + \left(\frac{1}{\sqrt{2}} - \frac{1}{\sqrt{6}} \right) x_2 \\
\varsigma_{22} &= \left(\frac{1}{\sqrt{2}} - \frac{1}{\sqrt{6}} \right) x_1 - \left(\frac{1}{\sqrt{2}} + \frac{1}{\sqrt{6}} \right) x_2 \\
\varsigma_{33} &= \sqrt{2/3}\,(x_1 + x_2) \\
\varsigma_{23} &= \varsigma_{32} = x_3 \\
\varsigma_{31} &= \varsigma_{13} = x_4 \\
\varsigma_{12} &= \varsigma_{21} = x_5.
\end{aligned}
\qquad (A.3)
$$

Once the components of $\boldsymbol{\varsigma}$ are obtained, principal stresses and stress axes are determined by solving the eigenproblem of $\boldsymbol{\varsigma}$. Then, Φ is determined from the principal stresses.

Distance between stress states is defined as

$$\Theta = \cos^{-1} \left\{ \left[\mathbf{x}^{(1)} \right]^\top \mathbf{x}^{(2)} \right\}, \qquad (A.4)$$

where $\mathbf{x}^{(1)}$ and $\mathbf{x}^{(2)}$ are the 5-dimensional unit vectors representing the stress states (Yamaji and Sato, 2006). The braces in Eq. (A.4) contains the scalar products of the vectors. That is, Θ is the angle made by $\mathbf{x}^{(1)}$ and $\mathbf{x}^{(2)}$. Therefore, the distance has a value between 0 and 180°. Stress states with $\Theta = 0°$ are identical to each other. If stress states denoted by the tensors $\boldsymbol{\varsigma}^{(1)}$ and $\boldsymbol{\varsigma}^{(2)}$ has the distance 180°, they are opposite state of stress: $\boldsymbol{\varsigma}^{(1)} = -\boldsymbol{\varsigma}^{(2)}$. Namely, those stress states have interchanging σ_1- and σ_3-orientations and the stress ratios Φ and $1 - \Phi$.

References

References

Andre, A.-S., Sausse J., Lespinasse M., 2001. New approach for the quantification of paleostress magnitudes: application to the Soultz vein system (Rhine graben, France). Tectonophysics 336, 215–231. doi:10.1016/S0040-1951(01)00103-2.

Baer, G. Beyth, M., Reches, Z., 1994. Dikes emplaced into fractured basement, Timna Igneous Complex, Israel. Journal of Geophysical Research 99, 24039–24051. doi:10.1029/94JB02161.

Beeler, N., Simpson, R., Hickman, S., Lockner, D., 2000. Pore fluid pressure, apparent friction, and Coulomb failure, Journal of Geophysical Research 105, 25533–25542. doi:10.1029/2000JB900119.

Bingham, C., 1974. An antipodally symmetric distribution on the sphere. Annals of Statistics 2, 1201–1225. doi:10.1214/aos/1176342874.

Bishop, A.W., 1966. The strength of soils as engineering materials. Géotechnique 16, 91–130. doi:10.1680/geot.1966.16.2.91.

Blenkinsop, T.G., 2008. Relationships between faults, extension fractures and veins, and stress. Journal of Structural Geology 30, 622–632. doi:10.1016/j.sg.2008.01.008.

Bonnet, E., Bour, O., Odling, N.E., Davy, P., Main, I., Cowie, P., Berkowitz, B., 2001. Scaling of fracture systems in geological media. Reviews of Geophysics 39, 347–383. doi:10.1029/1999RG000074.

Borradaile, G.J., 2003. Statistics of Earth Science Data: Their Distribution in Time, Space and Orientation. Springer, Berlin.

Delaney, P.T., Pollard, D.D., Zioney, J.I., McKee, E.H., 1986. Field relations between dikes and joints: emplacement processes and paleostress analysis. Journal of Geophysical Research 91, 4920–4983. doi:10.1029/JB091iB05p04920.

Dupin, J.-M., Sassi, W., Angelier, J., 1993. Homogeneous stress hypothesis and actual fault slip: a distinct element analysis. Journal of Structural Geology 15, 1033–1043. doi:10.1016/0191-8141(93)90175-A.

Geological Survey of Japan, 1992. Geological Map of Japan. Geological Survey of Japan, Third Edition, scale 1:1,000,000.

Gudmundsson, A., 1999. Fluid pressure and stress drop in fault zones. Geophysical Research Letters 26, 115–118. doi:10.1029/1998GL900228.

Hikichi, G.-Y., Yamaji, A., 2008. Paleostress analysis in metallogenic areas: the case of Nagano area, southern Kyushu, Japan. Journal of the Geological Society of Japan 114, 540–545.

Hood, S.D., Nelson, C.S., Kamp, P.J.J., 2003. Modification of fracture porosity by multiphase vein mineralization in an Oligocene nontropical carbonate reservoir, Taranaki Basin, New Zealand. American Association of Petroleum Geologists Bulletin 87, 1575–1597. doi:10.1306/06040301103.

Ikeda, T., 1962. Geology and ore deposits of the Okuchi Gold Mine, Kyushu: the fissure System of No. 3 Vein. Kyushu Kozan Gakkaishi 8, 35–338.

Izawa, E., 2004. The distribution map of volcanic rock and gold deposit in Hokusatsu. Chishitsu News 599, Photogravure.

Izawa, E., Urashima, Y., 2001. Quaternary gold mineralization and its geologic environments in Kyushu, Japan. In: Feebrey, C.A., Hayashi, T., and Taguchi, S. (Eds.), Epithermal gold mineralization and modern analogues, Kyushu, Japan, SEG Guidebook Series (CD-ROM) 34, 1–9.

Izawa, E., Watanabe, K., 2001. Overview of epithermal gold mineralization in Kyushu, Japan. In: Feebrey, C.A., Hayashi, T., and Taguchi, S. (Eds.), Epithermal gold mineralization and modern analogues, Kyushu, Japan, SEG Guidebook Series (CD-ROM) 34, 11–15.

Izawa, E., Yoshida, T., Sakai, T., 1981. Fluid inclusion studies on the gold-silver quartz veins at Kushikino, Kagoshima, Japan. Mining Geology, Special Issue 10, 25–34.

Izawa, E., Zeng, N., 2001. Kushikino gold mineralization in a Pliocene volcanic region, Kyushu, Japan. In: Feebrey, C.A., Hayashi, T., and Taguchi, S. (Eds.), Epithermal gold mineralization and modern analogues, Kyushu, Japan, SEG Guidebook Series (CD-ROM) 34, 53–60.

Jolly, R.J.H., Sanderson, D.J., 1997. A Mohr circle construction for the opening of a pre-existing fracture. Journal of Structural Geology 19, 887–892. doi:10.1016/S0191-8141(97)00014-X.

Kervyn, M., Ernst, G.G.J., van Wyk de Vries, B., Mathieu, L., Jacobs, P., 2008. Volcano load control on dyke propagation and vent distribution: insights from analogue modeling. Journal of Geophysical Research 114, B03401. doi:10.1029/2008JB005653

Love, J.J., 2007. Bingham statistics. In: Gubbins, D., Herrero-Bervira, E. (Eds.), Encyclopedia of Geomagnetism and Paleomagnetism, Springer, Dordrecht. 45–47.

Matsutoya, S., 1967. Structural features of Kushikino mine and its relation to the regional geologic structure of southwestern Kyushu. Kozan Chishitsu 17, 139–150.

Mazzarini, F., Isola, I., 2007. Hydraulic connection and fluid overpressure in upper crustal rocks: Evidence from the geometry and spatial distribution of veins at Botrona quarry, southern Tuscany, Italy. Journal of Structural Geology 29, 1386–1399. doi:10.1016/j.jsg.2007.02.016.

Mazzarini, F., Musumeci, G., 2008. Hydrofracturing-related sill and dyke emplacement at shallow crustal levels: the Eastern Elba Dyke Complex, Italy. In: Thomson, K., Petford, N. (Eds.), Structure and Emplacement of High-Level Magmatic Systems, Geological Society of London, Special Publications 203, 121–129. doi:10.1144/SP302.9.

McKeagney, C.J., Boulter, C.A., Jolly, R.J.H., Foster, R.P., 2004. 3-D Mohr circle analysis of vein opening, Indiama lode-gold deposit, Zimbabwe: implications for exploration. Journal of Structural Geology 26, 1275–1291, doi:10.1016/j.jsg.2003.11.001.

McKinstry, H.E., 1948. Mining Geology. Prentice-Hall, New York.

Miller, S.A., Collettini, C., Chiaraluce, L., Cocco, M., Barchi, M., Kaus, B.J.P., 2004. Aftershocks driven by a high-pressure CO_2 source at depth. Nature 427, 724–727, doi:10.1038/nature02251.

Ministry of International Trace and Industry, 1979. Report of Regional Geological Survey: previous Hokusatsu-Kushikino Area, Showa 53 (1978) Fiscal Year. Ministry of International Trade and Industry, Tokyo.

Mogi, K., 1958. Relations between the eruptions of various volcanoes and the deformation of the ground surfaces around them. Bulletin of Earthquake Research Institute, University of Tokyo, 36, 99–134.

Morishita, Y., Teraoka, Y., 1996. Boundary between the Chichibu and Shimanto terrains and hydrothermal activities in the Kushikino area, southwestern Kyushu. Resource Geology 46, 189–195.

Newhouse, W.H., 1942. Ore Deposits as Related to Structural Features. Princeton University Press, Princeton, New Jersey.

Pascal, C., 2002. Interaction of faults and perturbation of slip: influence of anisotropic stress states in the presence of fault friction and comparison between Wallace-Bott and 3D distinct element models. Tectonophysics 356, 307–322. doi:10.1016/S0040-1951(02)00413-4.

Pollard, D.D., Saltzer, S.D., Rubin, A.M., 1993. Stress inversion methods: are they based on faulty assumptions? Journal of Structural Geology 15, 1045–1054. doi:10.1016/0191-8141(93)90176-B.

Pyrak-Nolte, L.J., Morris, J.P., 2000. Single fractures under normal stress: The relation between fracture specific stiffness and fluid flow. International Journal of Rock Mechanics and Mining Sciences 37, 245–262. doi:10.1016/S1365-1609(99)00104-5.

Roberts, S., Sanderson, D.J., Gumiel, P., 1999. Fractal analysis and percolation properties of veins. In: McCaffrey, K.J.W., Lonergan, L., Wilkinson, J.J. (Eds.), Fractures, Fluid Flow and Mineralization, Geological Society of London, Special Publications 155, 7–16.

doi:10.1144/GSL.SP.1999.155.01.03.

Sanematsu, K., Watanabe, K., Duncan, R.A., Izawa, E., 2006. The history of vein formation determined by $^{40}Ar/^{39}Ar$ dating of adularia in the Hokusen-1 vein at the Hishikari epithermal gold deposit, Japan. Economic Geology 101, 685–698. doi:10.2113/gsecongeo.101.3.685.

Sato, K., Yamaji, A., 2006. Embedding stress difference in parameter space for stress tensor inversion. Journal of Structural Geology 28, 957–971. doi:10.1016/j.jsg.2006.03.004.

Sekine, R., Izawa, E., Watanabe, K., 2002. Timing of Fracture Formation and Duration of Mineralization at the Hishikari Deposit, Southern Kyushu, Japan. Resource Geology 52, 395–404. doi:10.1111/j.1751-3928.2002.tb00149.x.

Shiobara, M., Yoshikawa, 1958. The fissure system of the Kushikino mine, Kyushu, Japan. Kozan Chishitsu 8, 1–11.

Shipton, Z.K., Evans, J.P., Kirschner, D., Kolesar, P.T., Williams, A.P., Heath, J., 2004. Analysis of CO_2 leakage through 'low-permeability' faults from natural reservoirs in the Colorado Plateau, east-central Utah. In: Baines, S.J., Worden, R.H. (Eds.), Geological Storage of Carbon Dioxide, Geological Society, London, Special Publications 233, 43–58.

Sibson, R.H., 1987. Earthquake rupturing as a mineralizing agent in hydrothermal systems. Geology 15, 701–704. doi:10.1130/0091-7613.

Sibson, R.H., 1996. Structural permeability of fluid-driven fault-fracture meshes. Journal of Structural Geology 18, 1031–1042. doi:10.1016/0191-8141(96)00032-6.

Sibson, R.H., 2000. Fluid involvement in normal faulting. Journal of Geodynamics 29, 469–499, doi:10.1016/S0264-3707(99)00042-3.

Sillitoe, R.H., Hedenquist, J.W., 2003. Linkages between volcanotectonic settings, ore-fluid compositions, and epithermal precious metal deposits. In: Simmons, S.F., Graham, I. (Eds.), Volcanic, Geothermal, and Ore-Forming Fluids: Rulers and Witnesses of Processes within the Earth, Society for Economic Geologists, Special Publication 10, 315–343.

Stowell, J.F.W., Watson, A.P., Hudson, N.F.C., 1999. Geometry and population systematics of a quartz vein set, Holy Island, Angelesy, North Wales. In: McCaffrey, K.J.W., Lonergan, L., Wilkinson, J.J. (Eds.), Fractures, Fluid Flow and Mineralization, Geological Society of London, Special Publications 155, 17–33. doi:10.1144/GSL.SP.1999.155.01.04.

Sorkhabi, R., 2005. Gechemical signatures of fluid flow in thrust sheets: fluid-inclusion and stable isotope studies of calcite veins in western Wyoming. In: Sorkhabi, R., Tsuji, Y. (Eds.), Faults, Fluid Flow, and Petroleum Traps, American Association of Petroleum Geologists, Tursa, 251–267. doi:10.1306/1033727M853128.

Tamagawa, T., Pollard, D.D., 2008. Fracture permeability created by perturbed stress fields around active faults in a fractured basement reservoir. American Association of Petroleum Geologists Bulletin 92, 743–764. doi:10.1306/02050807013.

Tanaka, H., 1999. Circular asymmetry of the paleomagnetic directions observed at low latitude volcanic sites. Earth, Planets and Space 51, 1279–1286.

Uehara, S., Shimamoto, T., 2008. Contact analysis and permeability measurements of polished fracture surfaces in Sambagawa metapelitic schists and Ryoke mylonites from the Median Tectonic Line, Japan. Journal of Geophysical Research 114, B04205. doi:10.1029/2008JB005744.

Uto, T., Imai, A., Yamato, Y., 2001. Horizontal strain rate in relation to vein formation of the Hishikari gold deposits, southern Kyushu, Japan. Resource Geology 51, 7–18. doi:10.1111/j.1751-3928.2001.tb00077.

van den Bos, A., 2007. Parameter Estimation for Scientists and Engineers. Wiley, Hoboken.

Yamaji, A., 2003. Slab rollback suggested by latest Miocene to Pliocene forearc stress and migration of volcanic front in southern Kyushu, northern Ryukyu arc. Tectonophysics 364, 9–24, doi:10.1016/S0040-1951(03)00047-7.

Yamaji, A., Hase, Y., Torii, M., 2003. Paleostresses inferred from mesoscale faults in the Late Pliocene Hitoyoshi Formation; implications for the formation of vein-type ore deposits in southern Kyushu, Japan. Shigen Chishitsu 53, 217–225.

Yamaji, A., Sato, K., 2006. Distances for the solutions of stress tensor inversion in relation to misfit angles that accompany the solutions. Geophysical Journal International 167, 913–942. doi:10.1111/j.1365-246X.2006.03188.x

Yamaji, A., Yoshida, T., 1998. Multiple tectonic events in the Miocene Japan arc: the Heike microplate hypothesis. Journal of Mineralogy, Petrology and Economic Geology 93, 389–408. doi:10.2465/ganko.93.389.

11